BACKSCATTERING EFFECTS FOR DISCRETE RANDOM MEDIA: THEORETICAL RESULTS

VICTOR TISHKOVETS,[1] PAVEL LITVINOV,[1]
ELENA PETROVA,[2] KLAUS JOCKERS,[3] AND
MICHAEL MISHCHENKO[4]

[1]*Institute of Radioastronomy of NASU, 4 Chervonopraporna St., Kharkiv, Ukraine*
[2]*Space Research Institute of RAS, Profsoyuznaya 84/32, Moscow 117979, Russia*
[3]*Max-Planck-Institute for Aeronomy, Katlenburg-Lindau, D-37191, Germany*
[4]*NASA Goddard Institute for Space Studies, 2880 Broadway, New York, NY 10025, USA*

Abstract. The effect of enhanced backscattering of light from discrete random media, often referred to as the coherent photometric opposition effect (or weak photon localization), is a remarkable optical phenomenon that is being actively studied. When the incident light is unpolarized, the opposition intensity peak can be accompanied by the so-called opposition polarization effect, which manifests itself as a sharp asymmetric negative-polarization feature at small phase angles. The optical phenomenon that causes these effects is the constructive interference of multiply scattered waves propagating along the same light-scattering paths in a medium but in opposite directions. The theoretical description of multiple scattering becomes more complicated for closely packed media because of potentially significant near-field effects that can significantly depress the photometric opposition peak and increase the depth of the negative-polarization feature. In this chapter, we discuss the opposition effects for semi-infinite sparse scattering media and study their dependence on concentration and microphysical properties of the constituent scatterers. Manifestations of the near-field interactions are illustrated by theoretical calculations for randomly oriented clusters of spherical particles.

1. Introduction

The phenomenon of electromagnetic scattering and absorption is widely exploited in remote-sensing and laboratory characterization of various objects

G. Videen, Ya. Yatskiv and M. Mishchenko (eds.),
Photopolarimetry in Remote Sensing, pp. 221–242.

[1–14]. Calculations of different characteristics of radiation scattered by discrete random media are important in atmospheric optics, astrophysics, biophysics, and many other areas of science and engineering. More often than not, multiple-scattering effects on the characteristics of the measured detector response must be taken into account. In many cases measurements of angular dependencies of the emerging radiation demonstrate a backscattering enhancement in the form of a sharp peak of intensity centered at exactly the backscattering direction. This effect is also known as weak photon localization or the coherent opposition effect. In the case of unpolarized incident light, it can be accompanied by the so-called opposition polarization effect in the form of a branch of negative linear polarization limited to a narrow range of backscattering angles [8,9,12,14]. Presently, both effects are explained as the result of constructive interference of multiply scattered waves propagating inside the medium along direct and reverse trajectories [1–13].

The coherent backscattering effect was first predicted theoretically in studies of propagation of electromagnetic waves in turbulent plasmas [15]. Then it has been analyzed in numerous experimental and theoretical studies (see, e.g., [16–18] and references therein). The strong dependence of the angular width of the interference peak on the particle number density has been demonstrated both experimentally and theoretically [1–3]. However, only recently rigorous formulas describing the opposition effects have been derived in the particular case of normal incidence of light on a plane-parallel layer of a sparse discrete random medium. Specifically, a complete analytical solution for nonabsorbing, randomly positioned Rayleigh scatterers has been obtained in [19–21]. The rigorous approach was later extended to randomly positioned and randomly oriented particles with arbitrary sizes, shapes, and refractive indices [22]. A more general case of oblique illumination was analytically described in [23]. Numerical results obtained in the double-scattering approximation revealed a significant dependence of the characteristics of the opposition effects on particle microphysical properties [18,24,25].

Theoretical consideration of multiple light scattering by a closely packed medium is complicated by potentially significant near-field effects [26–28]. Indeed, the scattered electromagnetic wave in the close vicinity of the scatterer is strongly inhomogeneous. The analysis of scattering of this wave by an adjacent particle requires more sophisticated techniques than those used to address the problem of scattering of a plane electromagnetic wave.

In this chapter, we discuss the opposition effects for sparse media and closely packed systems of particles. Section 2 summarizes the basic equations describing the scattering of light by systems of spherical particles. Specific differences in the description of light scattering by closely packed and by sparse systems of particles will be discussed. In section 3, equations for the reflection matrix of a layer of sparse medium are given. Numerical examples illustrate considerable dependence of the opposition effects on microscopic

characteristics of the constituent scatterers. In section 4, the near-field effects and their manifestations in light scattering by randomly oriented clusters of spherical particles will be qualitatively considered.

2. Basic definitions and equations

Over the past few decades, the approach based on the theory of electromagnetic scattering by particle ensembles (clusters) has become quite popular in analyzing the problem of light scattering by discrete random media. We use the theory of electromagnetic scattering by ensembles of spherical particles [29] in order to derive equations describing the process of multiple scattering in discrete random media. An assumption of particle sphericity is not crucial. However, it allows us to avoid more complex and cumbersome calculations. The generalization of the results thus obtained to randomly oriented nonspherical particles forming a low-density medium can be achieved rather easily [22,23].

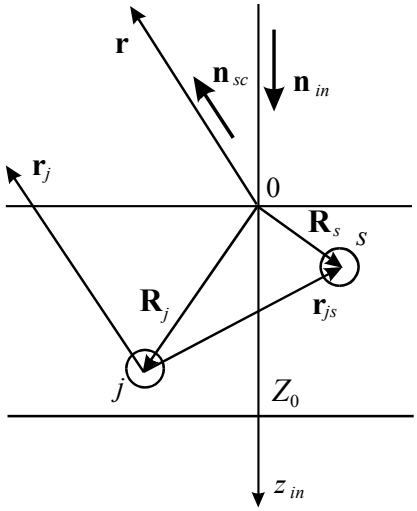

Figure 1: Scattering geometry (see text).

Consider a discrete random medium in the form of a homogeneous and isotropic layer consisting of randomly positioned spherical particles and denote by Z_0 its geometrical thickness. The scattering geometry is specified using the coordinate system shown in Fig. 1. An incident plane wave propagates along the z_{in}-axis of a coordinate system $\hat{\mathbf{n}}_{in}$. Throughout the paper, bold letters with carets $\hat{\mathbf{n}}_i$ denote right-handed coordinate systems (x_i, y_i, z_i) with the z_i-axes along the unit vectors $\mathbf{n}_i$. Coordinates of scatterers are determined in the coordinate system $\hat{\mathbf{n}}_{in}$ whose xy plane coincides with the upper boundary of the medium. The scattered wave propagates along the z_{sc}-axis of the coordinate

system $\hat{\mathbf{n}}_{sc}$. The rotation from $\hat{\mathbf{n}}_{in}$ to $\hat{\mathbf{n}}_{sc}$ is determined by the Euler angles $\varphi, \vartheta, \gamma$.

It is convenient to describe wave scattering by using the circular-polarization basis, in which the incident wave can be written as

$$\mathbf{E}_n^{(0)} = \mathbf{e}_n(\hat{\mathbf{n}}_{in}) \exp(ik\mathbf{n}_{in}\mathbf{r}), \tag{1}$$

where $n = \pm 1$, $k = 2\pi/\lambda$, λ is the wavelength, and $\mathbf{e}_n(\hat{\mathbf{n}}_{in})$ is a covariant spherical basis vector [30] in the coordinate system $\hat{\mathbf{n}}_{in}$. When $n = 1$, the direction of rotation of the electric vector of the wave (1) corresponds to the clockwise direction when looking in the direction of the vector $\mathbf{n}_{in}$. The linearity of the Maxwell equations and boundary conditions allows one to define the amplitude scattering matrix of the entire layer T_{pn} as

$$\begin{pmatrix} E_1 \\ E_{-1} \end{pmatrix} = \frac{\exp(ikr)}{-ikr} \begin{pmatrix} T_{11} & T_{1-1} \\ T_{-11} & T_{-1-1} \end{pmatrix} \begin{pmatrix} E_1^0 \\ E_{-1}^0 \end{pmatrix}, \tag{2}$$

where r is the distance from the origin of the coordinate system $\hat{\mathbf{n}}_{in}$ to the observation point, and then to express it in the form

$$T_{pn} = \sum_j t_{pn}^{(j)}. \tag{3}$$

Here $t_{pn}^{(j)}$ is the 2×2 amplitude scattering matrix [29] of the j th scatterer. Equation (2) assumes that all linear dimensions of the medium are small relative to r. The 4×4 scattering matrix **S**, which transforms the Stokes parameters of the incident wave into those of the scattered light [29], is defined by the following expression:

$$S_{pn\mu\nu} = \langle \sum_j t_{pn}^{(j)} t_{\mu\nu}^{*(j)} \rangle + \langle \sum_{j,\sigma\neq j} t_{pn}^{(j)} t_{\mu\nu}^{*(\sigma)} \rangle, \tag{4}$$

where the angular brackets denote ensemble averaging, the indices take on the values $p, n, \mu, \nu = \pm 1$, and the asterisk denotes complex conjugation.

We use the standard theory of light scattering by a system of spherical particles to derive the requisite equations. In this case the field scattered by the j th particle can be expressed in the form [22,23,29]

$$\mathbf{E}^{(j)} = \frac{\exp(ikr_j)}{-ikr_j} \sum_{pLM} \frac{2L+1}{2} A_{LM}^{(jpn)} D_{Mp}^{*L}(\hat{\mathbf{n}}_{in}, \hat{\mathbf{n}}_{sc}) \mathbf{e}_p(\hat{\mathbf{n}}_{sc}). \tag{5}$$

Here the $D_{Mp}^{L}(\hat{\mathbf{n}}_{in}, \hat{\mathbf{n}}_{sc}) = \exp(-iM\varphi)\, d_{Mp}^{L}(\vartheta) \exp(-ip\gamma)$ are Wigner D functions [30], r_j is the distance from particle j to the observation point, $\mathbf{n}_{sc}$ is the unit vector in the scattering direction, $\mathbf{e}_p(\hat{\mathbf{n}}_{sc})$ is a covariant spherical

basis vector in the coordinate system $\hat{\mathbf{n}}_{sc}$. It is assumed here that the scattering direction is the same for all particles of the medium.

The coefficients $A_{LM}^{(jpn)}$ are determined by the system of equations [22,29]

$$A_{LM}^{(jpn)} = a_L^{(jpn)} \exp(ik\mathbf{n}_{in}\mathbf{R}_j)\delta_{Mn} + \sum_{q,s\neq j} a_L^{(jpq)} \sum_{lm} A_{lm}^{(sqn)} H_{LMlm}^{(q)}(\hat{\mathbf{n}}_{in}, \hat{\mathbf{n}}_{sj}), \qquad (6)$$

where $a_L^{(jpn)} = a_L^{(j)} + pnb_L^{(j)}$, $a_L^{(j)}$ and $b_L^{(j)}$ are the Lorenz-Mie coefficients [29], $q = \pm 1$, $\mathbf{R}_j$ is the radius-vector of particle j (Fig.1), $\hat{\mathbf{n}}_{sj}$ is the coordinate system with the z_{sj} axis along the vector $\mathbf{r}_{sj}$, and the $H_{LMlm}^{(q)}(\hat{\mathbf{n}}_{in}, \hat{\mathbf{n}}_{sj})$ are the coefficients of the addition theorem for the vector Helmholtz harmonics [22,26,31]

$$H_{LMlm}^{(q)}(\hat{\mathbf{n}}_{in}, \hat{\mathbf{n}}_{sj}) = \frac{2l+1}{2}(-1)^m \sum_{l_1 m_1} i^{-l_1} h_{l_1}(kr_{js}) D_{m_1 0}^{l_1}(\hat{\mathbf{n}}_{in}, \hat{\mathbf{n}}_{sj}) C_{LMl-m}^{l_1 m_1} C_{Lql-q}^{l_1 0}. \qquad (7)$$

Here $h_l(x)$ is the Hankel spherical function of the first kind, and the Cs are the Clebsch-Gordan coefficients [30].

To determine the matrix $t_{pn}^{(j)}$, let us introduce the basis vectors $\mathbf{e}_\perp$ and $\mathbf{e}_\parallel$ with respect to the plane through the vectors $\mathbf{n}_{in}$ and $\mathbf{n}_{sc}$. The vector $\mathbf{e}_\perp$ is perpendicular to the reference planes, whereas the vector $\mathbf{e}_\parallel$ is parallel to them. Transforming these vectors into spherical basis vectors yields the contravariant spherical basis vectors [30] $\mathbf{e}^n(\hat{\mathbf{n}}_{in})$ and $\mathbf{e}^p(\hat{\mathbf{n}}_{sc})$, which are rotated with respect to the vectors $\mathbf{e}_n(\hat{\mathbf{n}}_{in})$ and $\mathbf{e}_p(\hat{\mathbf{n}}_{sc})$ through the angles φ and $-\gamma$, respectively. We, therefore, get from Eqs. (2) and (5)

$$t_{pn}^{(j)} = \exp(-ik\mathbf{n}_{sc}\mathbf{R}_j - in\varphi - ip\gamma) \sum_{LM} \frac{2L+1}{2} A_{LM}^{(jpn)} D_{Mp}^{*L}(\hat{\mathbf{n}}_{in}, \hat{\mathbf{n}}_{sc}). \qquad (8)$$

The solution of the system of equations (6) can be obtained by iteration. This representation of the solution corresponds to the expansion of the coefficients $A_{LM}^{(jpn)}$ in a multiple-scattering series. The first two terms of this series are

$$A_{LM}^{(jpn)} = a_L^{(jpn)} \exp(ik\mathbf{n}_{in}\mathbf{R}_j)\delta_{Mn} + \sum_q a_L^{(jpq)} \sum_{slm} a_l^{(sqn)} H_{LMlm}^{(q)}(\hat{\mathbf{n}}_{in}, \hat{\mathbf{n}}_{sj}) \exp(ik\mathbf{n}_{in}\mathbf{R}_s)\delta_{mn} + \dots . \qquad (9)$$

By inserting the series (9) into Eq. (8), writing the same series for the incident wave with the initial polarization ν and scattered polarization μ, and calculating the matrix (4) we will obtain the series corresponding to various scenarios of wave scattering. Let us combine the terms corresponding to the

same scattering scenario. Then the matrix (4) can be represented as

$$S_{pn\mu\nu} = S^{1}_{pn\mu\nu} + S^{\mathrm{L}}_{pn\mu\nu} + S^{\mathrm{C}}_{pn\mu\nu} + S^{\mathrm{O}}_{pn\mu\nu}. \tag{10}$$

Here the matrix $\mathbf{S}^1$ corresponds to the first-order scattering, including the interference of singly scattered waves. The matrix $\mathbf{S}^{\mathrm{L}}$ is the sum of all scattering orders corresponding to the case when both waves propagate along the same path in the same direction, thereby describing incoherent scattering. The matrix $\mathbf{S}^{\mathrm{C}}$ is the sum of all scattering orders corresponding to the case when both waves propagate along the same path, but in opposite directions. In the backscattering region, the interference of such waves is constructive and results in the opposition effects. The matrix $\mathbf{S}^{\mathrm{O}}$ corresponds to the rest of scattering contributions, including the interference of waves scattered once and twice, twice and three times, etc.

Thus, the calculation of the matrix (4) reduces to the calculation of the matrices $\mathbf{S}^1$, $\mathbf{S}^{\mathrm{L}}$, $\mathbf{S}^{\mathrm{C}}$, and $\mathbf{S}^{\mathrm{O}}$. It is very difficult to calculate all these matrices for closely packed media comprising scatterers comparable to the wavelength. In this case, the matrix $\mathbf{S}^{\mathrm{O}}$ can contribute significantly to the matrix (4), and all the matrices must be calculated with the coefficients of the addition theorem in the form (7). These coefficients describe all peculiarities of the waves in the vicinity of the scatterers including the near-field effects. For low-density media, when the distances between the particles $r_{js} >> \tilde{a}_j$, $\tilde{a}_s$ (where the $\tilde{a}_j$ and $\tilde{a}_s$ are the radii of particles j and s, respectively), these coefficients are

$$H^{(q)}_{LMlm}(\hat{\mathbf{n}}_{in}, \hat{\mathbf{n}}_{sj}) = \frac{2l+1}{2} \frac{\exp(ikr_{js})}{-ikr_{js}} D^{L}_{Mq}(\hat{\mathbf{n}}_{in}, \hat{\mathbf{n}}_{sj}) D^{*l}_{mq}(\hat{\mathbf{n}}_{in}, \hat{\mathbf{n}}_{sj}). \tag{11}$$

If the scatterers are randomly positioned and $r_{js} >> \lambda$, then the matrix $\mathbf{S}^{\mathrm{O}}$ vanishes, and Eq. (10) takes the form

$$S_{pn\mu\nu} = S^{1}_{pn\mu\nu} + S^{\mathrm{L}}_{pn\mu\nu} + S^{\mathrm{C}}_{pn\mu\nu}. \tag{12}$$

In the next section, we will give the equations to calculate the matrix (12) corresponding to the reflection of radiation from a plane-parallel layer. In solving these equations numerically, our main interest will be in the dependence of the opposition effects on microphysical properties of the medium such as particle size, refractive index, and concentration.

3. Backscattering by a sparse plane-parallel layer

In this section, we consider multiple scattering by a plane-parallel layer consisting of discrete, randomly positioned scatterers of arbitrary shape and in random orientation. The incident wave is assumed to propagate normally to the boundary of the medium. A derivation of the equations describing the

matrix (12) in this case was given in [22]. The more general case of oblique illumination is considered in [23]. In the circular polarization basis, the equations for the matrices $\mathbf{S}^1$ and $\mathbf{S}^L$, defined per unit area of the boundary, take the following form:

$$S^1_{pn\mu\nu} + S^L_{pn\mu\nu} = \frac{\eta}{k}\sum_l d^l_{M_0N_0}(\vartheta)\int_0^{kZ_0}\exp\left(2z\frac{\mathrm{Im}(\varepsilon)}{\cos\vartheta}\right)\alpha_l^{(z)(pn)(\mu\nu)}dz, \qquad (13)$$

where η is the particle number density, $p,n,\mu,\nu = \pm 1$, $M_0 = \nu - n$, $N_0 = \mu - p$, ϑ is the scattering angle (the angle between the incidence and scattering directions), and ε is the complex effective refractive index of the medium. The expansion coefficients $\alpha_L^{(z)(pn)(\mu\nu)}$ are determined from the system of equations

$$\alpha_L^{(z)(pn)(\mu\nu)} = \chi_L^{(pn)(\mu\nu)}\exp(-\tau_z) + \frac{2\pi\eta}{k^3}\sum_{qq_1}\chi_L^{(pq)(\mu q_1)} \times\int\sum_l \alpha_L^{(y)(qn)(q_1\nu)}\exp(-\tau_\rho)d^L_{M_0N}(\omega)d^l_{M_0N}(\omega)d\rho\sin\omega d\omega, \qquad (14)$$

where ρ,ω are polar coordinates of the integration point with respect to the point z, the angle ω is measured relative to the backscattering direction, $\tau_x = 2\,\mathrm{Im}(\varepsilon)x$, $N = q_1 - q$ ($q,q_1 = \pm 1$), and $y = z - \rho\cos\omega$. The upper integration limit over ρ is equal to $z/\cos\omega$ for $\omega < \pi/2$ and to $(z - Z_0k)/\cos\omega$ for $\omega > \pi/2$. The $\chi_L^{(pn)(\mu\nu)}$ are the coefficients in the expansion of the individual-particle scattering matrix [29] in the Wigner *d* functions [30]. Equations (13) and (14) are equivalent to the vector radiative transfer equation in the circular-polarization basis.

The corresponding equations for matrix $\mathbf{S}^C$ are as follows:

$$S^C_{pn\nu\mu} = \frac{2\pi\eta^2}{k^4}\sum_{qq_1LM}(-1)^L\zeta_{LM}^{*(q_1\mu)(qp)}\int_0^{kZ_0}\beta_{LM}^{(z)(qn)(q_1\nu)}\exp(-\varepsilon_1 z)dz, \qquad (15)$$

where the matrix $\beta_{LM}^{(z)(pn)(\mu\nu)}$ is defined by system of equations

$$\beta_{LM}^{(z)(pn)(\mu\nu)} = B_{LM}^{(pn)(\mu\nu)}\exp(-\varepsilon_1^* z) + \frac{2\pi\eta}{k^3}\sum_{qq_1lm}\chi_l^{(pq)(\mu q_1)}i^{M-m}\int\beta_{lm}^{(y)(qn)(q_1\nu)} \times d^L_{MN_0}(\omega)d^l_{mN_0}(\omega)\exp(-\tau_\rho)J_{m-M}(\rho\sin\vartheta\sin\omega)d\rho\sin\omega d\omega. \qquad (16)$$

Here $\zeta_{LM}^{(pn)(\mu\nu)}$ are the coefficients in the expansion of the phase matrix elements [22–25] in Wigner *d* functions, $J_m(x)$ are Bessel functions,

$$\varepsilon_1 = \mathrm{Im}(\varepsilon)\left(1-\frac{1}{\cos\vartheta}\right)+i\left(\cos\vartheta+1\right)\left(\frac{\mathrm{Re}(\varepsilon)-1}{\cos\vartheta}+1\right), \qquad (17)$$

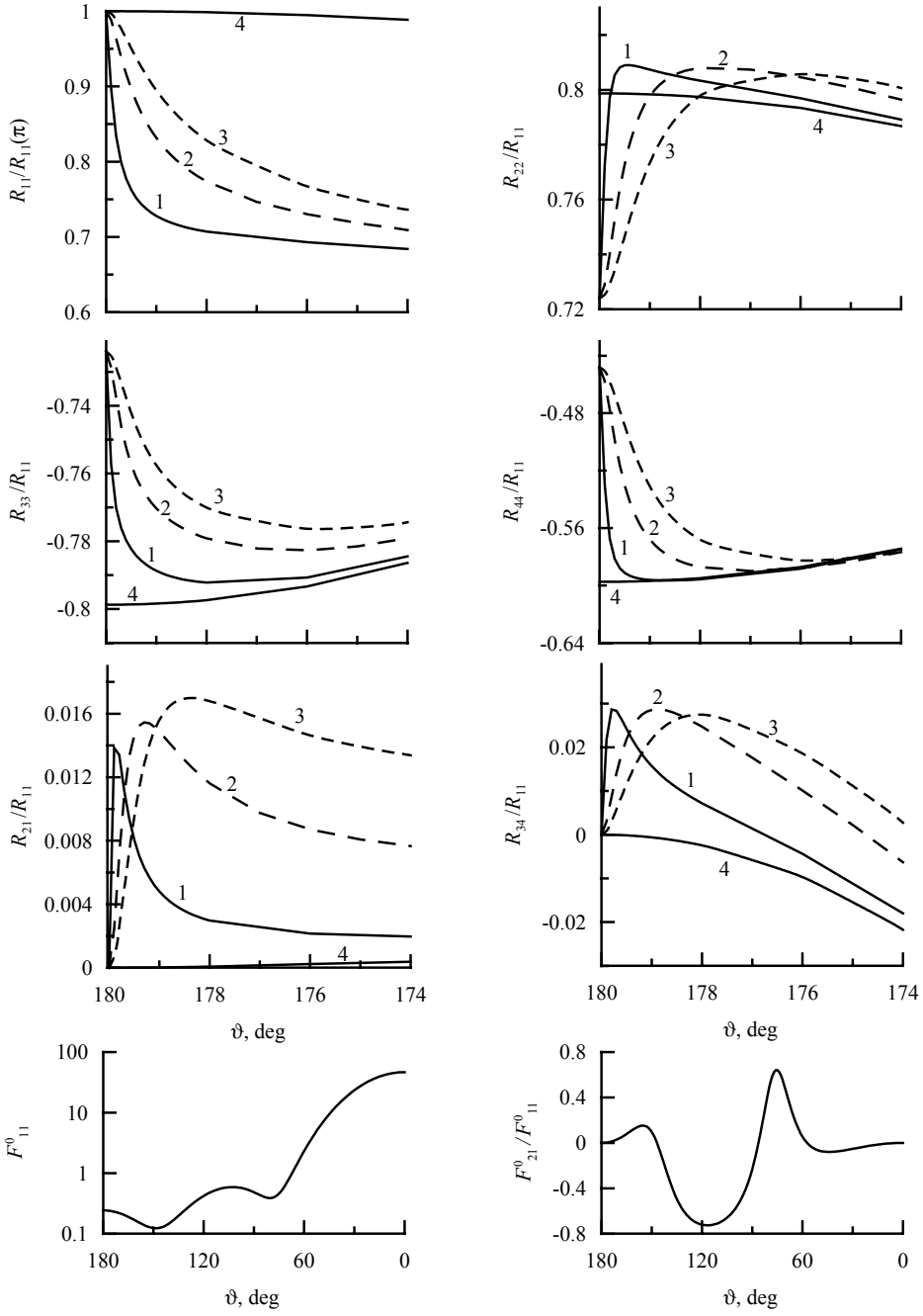

Figure 2: The angular dependence of the reflection matrix elements for a semi-infinite medium composed of spherical particles with $\tilde{x}=3$ and $\tilde{m}=1.35+0i$ for various values of the filling factor: 1) $\xi=0.001$, 2) $\xi=0.005$, 3) $\xi=0.01$, 4) the incoherent component. The F^0_{11} and F^0_{21} are scattering matrix elements for an individual scatterer.

$$B_{LM}^{(pn)(\mu\nu)} = \sum_{lm} \zeta_{lm}^{(pq)(\mu q_1)} i^{M-m} \int d_{MN_0}^{L}(\omega) d_{mN_0}^{l}(\omega) J_{m-M}(\rho \sin\vartheta \sin\omega)$$

$$\times \exp(-\tau_\rho + \rho\varepsilon_1^* \cos\omega) d\rho \sin\omega d\omega. \qquad (18)$$

The matrix $\mathbf{S}^{\mathrm{C}}$ describes the interference of the conjugate pairs of waves propagating along the same trajectories in the medium but in opposite directions, including looped trajectories.

Equations (13)–(18) are rigorous provided that any scatterer is located in the far-field zone of all other scatterers. They are valid for arbitrary particles in random orientation. It should be noted that in the case of the exact backscattering direction ($\vartheta = \pi$), the matrix $\mathbf{S}^{\mathrm{C}}$ can be obtained from the matrix $\mathbf{S}^{\mathrm{L}}$ using the equation $S_{pn\nu\mu}^{\mathrm{C}} = S_{pn\mu\nu}^{\mathrm{L}}$ [32].

The above equations for a semi-infinite medium can be solved numerically in the approximation of several scattering orders. All the calculations below will be given for the reflection matrix $\mathbf{R} = -\mathbf{S}/2k^2 \cos\vartheta$ in the linear-polarization basis. The transformation of the matrix (12) from the circular-polarization basis to the linear-polarization one can be found in [29]. The effective refractive index of the medium is given by $\varepsilon = 1 + i\eta C_{\mathrm{ext}}/2k$, where C_{ext} is the extinction cross section per particle [29].

Figure 2 depicts all nonzero elements of the reflection matrix in the double-scattering approximation for a semi-infinite layer composed of identical spherical particles. The particle size parameter is $\tilde{x} = 2\pi\tilde{a}/\lambda = 3$, where $\tilde{a}$ is the particle radius, and the particle refractive index is $\tilde{m} = 1.35 + 0i$. The results are shown for different values of the filling factor (packing density) $\xi = 4\pi\tilde{a}^3\eta/3$.

As seen from Fig. 2, the interference affects all elements of the reflection matrix. The linear dependence of the width of the intensity peak on the packing density (the R_{11} curves), which was discussed in theoretical and experimental studies (see [1–3] and references in [17]), is well noticeable. The examples given in Fig. 2 as well as other calculations not shown here reveal the same dependence on ξ in the other components of the coherent refection matrix. For instance, the angular position of the R_{21} and R_{34} extrema depends linearly on ξ if the corresponding matrix elements for the incoherent component depend weakly on ϑ . Otherwise, the superposition of the coherent and incoherent components disrupts this linear dependence [24].

Figure 3 demonstrates the dependence of the intensity and the degree of linear polarization of the reflected light on the particle properties and on the order of scattering. Since the effective refractive index of the medium is kept the same, the differences in the features of the opposition effects are caused by the differences in the microscopic characteristics of the scatterers. To explain the influence of the particle properties on the R_{11} element, let us consider the interference of doubly

scattered waves for two cases of scattering geometry. Let two particles be placed along the direction of the $\mathbf{n}_{in}$ vector in the first case and along the perpendicular direction in the second case. Then the phase difference for the waves propagating along the direct and reverse paths is proportional to $1+\cos\vartheta$ in the first case and to $\sin\vartheta$ in the second case. For $\vartheta\to\pi$, the difference for the first pair of particles is negligible, whereas for the second one it is proportional to $\pi-\vartheta$. In other words, the first pair produces a broader interference peak than the second one. Particles with $\tilde{x}=4.5$ scatter radiation more effectively in the forward and backward directions than particles with $\tilde{x}=3$ (compare curves 2, 3 and 1 of Fig. 3c). As a result, the width of the intensity peak for a medium composed of these particles is larger (compare curves 2, 3 and 1 of Fig. 3a). Particles with $\tilde{x}=4.5$ and $\tilde{m}=1.59+0i$ display a more symmetric phase function than those with $\tilde{x}=4.5$ and $\tilde{m}=1.35+0i$, and the peak for these particles is sharper.

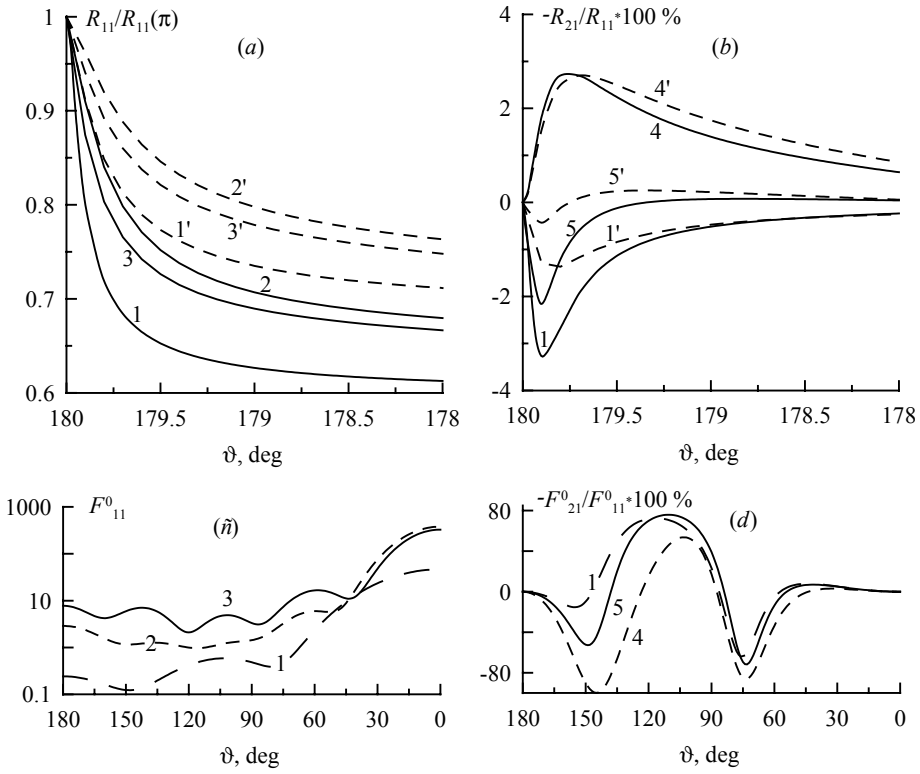

Figure 3: The dependence of the relative intensity (a) and the degree of linear polarization (b) on the particle properties and on the scattering order. The curve numbers correspond to the following parameters: 1) $\tilde{x}=3$, $\tilde{m}=1.35+0i$, $\xi=0.0012$; 2) $\tilde{x}=4.5$, $\tilde{m}=1.35+0i$, $\xi=0.001$; 3) $\tilde{x}=4.5$, $\tilde{m}=1.59+0i$, $\xi=0.001$; 4) $\tilde{x}=3$, $\tilde{m}=1.50+0i$, $\xi=0.0007$; 5) $\tilde{x}=3.1$, $\tilde{m}=1.35+0i$, $\xi=0.0011$. In all cases, $\mathrm{Im}(\varepsilon)=0.000286$. The dashed curves are for the double-scattering approximation, whereas the solid ones are computed with the account of the third-order scattering. The F_{11}^0 and F_{21}^0 are scattering matrix elements for an individual scatterer.

The results of Fig. 3(b) demonstrate that the state of polarization of the backscattered radiation is controlled strongly by the intensity and state of polarization of singly scattered radiation (i.e., by the angular profiles of F_{11}^0 and F_{21}^0). It is well known that positive polarization of light scattered by isolated particles leads to a negative-polarization feature in the backscattering direction [8,9]. The angular dependence of the polarization state for wavelength-sized spherical particles is much more complex and oscillatory [29]. The resulting interference of doubly scattered waves can result in positive polarization (curves 4 and 4') as well as in negative polarization (curves 1 and 1' and curves 5). Such behavior of polarization was analyzed in detail in [23,25]. The interference may lead to a more complex dependence of polarization on the scattering angle, with positive and negative polarization regions appearing simultaneously (curve 5' in Fig. 3b).

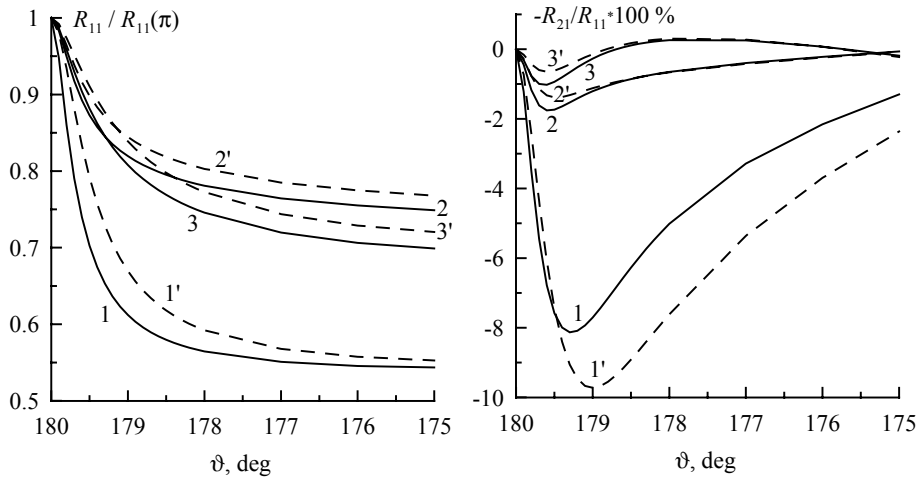

Figure 4: The same as in Fig.3 (a) and (b) but for the third-order-scattering approximation (dashed curves) and an approximate solution including all orders of scattering (solid curves). Curves 1 and 1': $\tilde{x}$ =3, $\tilde{m}$ =1.35+0.1i, ξ =0.0076; curves 2 and 2': $\tilde{x}$ =2, $\tilde{m}$ =1.4+0.5i, ξ =0.0048; curves 3 and 3': $\tilde{x}$ =3, $\tilde{m}$ =1.5+0.5i, ξ =0.0061. In all cases, $\mathrm{Im}(\varepsilon) = 0.002$.

As can be seen in Fig. 3, the angular range where the interference contributes noticeably to the scattered radiation is becoming narrower with increasing order of scattering (see also [3]). In Fig. 4 the results of the third-order-scattering approximation are compared with the results of an approximate calculation including all orders of scattering, as follows. The radiation coming to the particle from above is calculated exactly, and a part of radiation coming to the particle from below is calculated approximately, as if for an infinite medium. The errors of this approximation were estimated for the incoherent scattering term for particles with $\tilde{x} = 3$ and $\tilde{m} = 1.5 + 0.5i$ or

$\tilde{m} = 1.5 + 0.1i$ and do not exceed 10% and 15%, respectively. The explanation of the angular behavior of the intensity and polarization of the multiply scattered radiation is similar to that for the double- and third-order-scattering approximations.

All the results presented in this section were obtained in the approximation of quasi-homogeneous waves [16], which implies that any particle of the medium is in the wave zones of all other particles. This assumption allows the radiation reflected by the medium to be represented as a sum of the matrices (12) with the coefficients (11). Moreover, the characteristics of individual scattering particles, such as the scattering matrix [29], can be used in the calculations of multiply scattered waves. In closely packed media, a wave propagating from a scatterer to another one can be strongly inhomogeneous. This effect, which can significantly influence the opposition phenomena, will be the focus of the next section.

4. Opposition effects for closely packed systems of spherical particles

4.1. Near-field effects

The reflection matrix for a closely packed medium composed of wavelength-sized scatterers can be represented as a sum of matrices (10) with the coefficients of the addition theorem (7). These coefficients describe all the details of the field in the vicinity of any scatterer, including the near-field effects [26]. We will consider the manifestations of these effects qualitatively using the field configuration near a spherical scatterer as the simplest example.

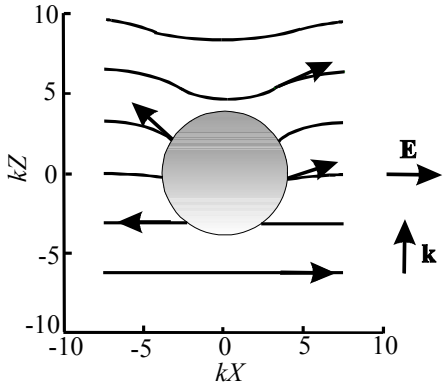

Figure 5: Surfaces of constant phase and directions of vectors **E** (sum of the incident and scattered waves) in the close vicinity of a spherical particle. The incident wave propagates along the *Z*-axis (indicated by the wave vector **k**) and is polarized along the *X*-axis. The particle size parameter is $\tilde{x}$ =4 and the refractive index is $\tilde{m} = 1.32 + 0.05i$.

In the immediate vicinity of an individual particle or a system of particles, the scattered wave is strongly inhomogeneous. For such a wave, surfaces of

constant phase and amplitude do not coincide, and the amplitude, polarization, and propagation directions depend on the location with respect to the scatterer. When the inhomogeneous wave excites another particle, the resulting scattered light can differ substantially from that predicted by the theory based on the consideration of only plane waves. In what follows, the effects caused by wave inhomogeneity will be referred to as near-field effects.

Direct calculations using the Lorentz–Mie theory for spherical particles show that the surfaces of constant phase of the total field are funnel-shaped in the vicinity of the particle (Fig. 5). Such near-field properties are typical for spherical particle with other size and refractive index [26,28].

Let us consider test Rayleigh particles surrounding a constituent particle (CP) of a particle aggregate and adopt a coordinate system in which the *Z*-axis is along the propagation direction of the incident wave, whereas the *XZ*-plane defines the scattering plane (Fig. 6). The incident field is assumed to be polarized in the scattering plane. If the test particles were far from the CP and far from each other, they would experience a homogeneous electromagnetic field (Fig. 6a). The dipole moment induced in the test particles would be along the *X*-axis. However, if the test particles are close to each other and to the CP, a dipole moment induced in test particles 1 and 3 has a non-zero component in the direction of wave propagation *Z* (Fig. 6b). At the same time, the *X*-component of the dipole moment is smaller than in the case of a large distance between the CP and the test particles.

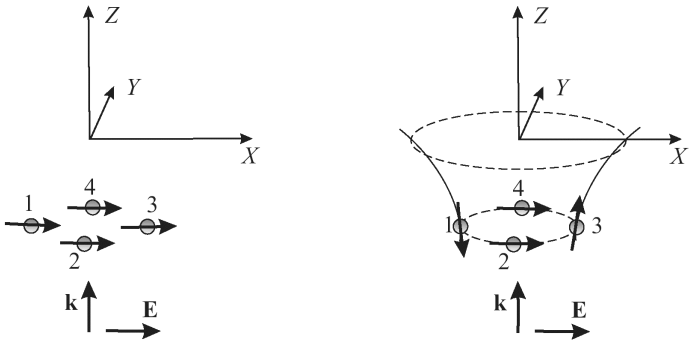

Figure 6: Light scattering by a system of dipoles excited by a homogeneous and an inhomogeneous wave. The incident wave propagates along the *Z*-axis and is polarized in the *XZ*-plane. a): The wave is homogeneous, and all dipole moments point in the *X*-direction. b): The wave is inhomogeneous because of the distortion of the wave front (see Fig. 5), and some dipole moments have a non-zero *Z* component.

The changes of the dipole moment induced by the high packing density do not depend on the polarization of the incident wave. If the latter were polarized perpendicularly to the scattering plane, the roles of test particles 1 and 3 and 2 and 4 would simply be interchanged, i. e. the gross changes of the induced

dipole moment would be the same and would only be caused by other test particles. Consideration of light scattering by an ensemble of test dipoles (without interference waves) shows the intensity at $\vartheta = 0$ and $\vartheta = \pi$ for Fig.6b less then for Fig.6a and vice versa at $\vartheta = \pi/2$. The angle dependence of the degree of linear polarization is bell-shaped and may be negative for Fig.6b, whereas for Fig.6a it is positive with maximum value 100% at $\vartheta = \pi/2$. In other words, the inhomogeneity of the wave in the particle vicinity and its interaction with neighboring scatterers will reduce the scattered intensity in the directions $\vartheta \approx 0$ and $\vartheta \approx \pi$ and lead to the appearance (or enhancement of already existing) negative polarization in the backscattering region.

An analogous analysis of scattering in a densely packed ensemble of particles using the other wavelength-sized CPs instead of the test Rayleigh scatterers requires the consideration of the gradient of the wave inhomogeneity. Unfortunately, this problem is far from being well-studied. We can only note the following. The zone of wave inhomogeneity extends to distances of the order of λ from the particle surface. Consequently, the near-field effects are essential only for CPs with sizes comparable to or less than λ and are negligible for larger particles. A closer examination of the near-field effects including simulation examples for various types of particles is performed in [26–28,34]. These examples display a complex dependence of the near-field effects on the particle properties and the scattering angle. In the first approximation, the effect of the rotation of the field vector, which is mainly caused by the radial component of the scattered field, is described by the interference of waves scattered once and twice. Its contribution strongly depends on the size and refractive index of the CPs, the distance between them, and the scattering angle.

4.2. Opposition effects for randomly oriented clusters of spherical particles

We illustrate the scattering phenomena described above using a bisphere as the simplest example. We assume that the bisphere consists of monomers with the size parameter $\tilde{x} = 1.49$. The complex refractive index of the monomers is $\tilde{m} = 1.80 + 0.01i$. A sphere with these optical parameters has neutral (near zero) polarization at scattering angles close to the backscattering direction and positive polarization elsewhere. In view of the preceding discussion of wave interference and near-field effects, this will allow us to demonstrate how the different optical phenomena contribute to intensity and polarization. To explain qualitatively all these phenomena, we restrict the analysis to the double-scattering approximation and use the formulas derived in [26]. The results are given in Fig. 7 computed for the case of touching spheres. Curves 1 correspond to a single particle. Curves 2 were computed by including the contributions of single scattering, incoherent double scattering, and the

interference of singly scattered light. Model 3 additionally takes into account the contribution of the interference of waves scattered twice, which leads to the backscattering enhancement of intensity and a weak negative branch in polarization. Model 4 includes all the components of model 3 plus the interference of singly and doubly scattered waves, i. e. all first- and second-order scattering terms. As compared to model 3, the intensity is reduced and the negative branch develops further. Curves 5 shows the exact solution.

Curves 2–5 are obtained by taking the near field effects into account [see Eqs. (7) and (10)]. In order to demonstrate what happens if these effects are ignored, we also show the curves derived for homogeneous waves [see Eqs. (11) and (12)], i.e., when the waves propagating from one particle to another are assumed to be spherical and have only tangential components of the field vector (curves 6). This approach was considered in [8,9]. It is evident that the homogeneous-wave approximation is invalid for touching monomers, i.e. the near-field effects must be taken into account in this case. As seen from Fig. 7, the interference contribution is essential for $\vartheta > 130°$ (compare the behavior of curves 2, 3, and 6), whereas the near-field effects influence a wider angular range (compare curves 4 and 3).

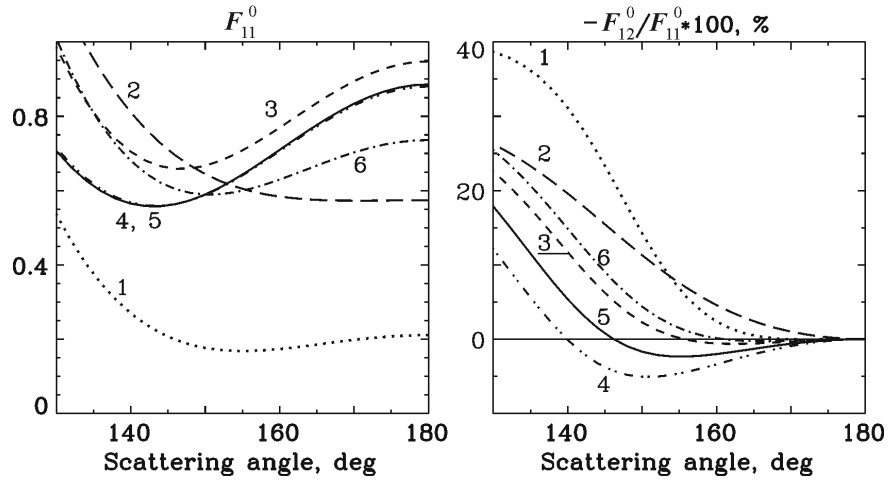

Figure 7: The contributions of interference and near-field effects in the backscattering region as demonstrated by the example of a bisphere. The curves correspond to the following models. Curves 1 (dots): calculations for single sphere; curves 2–6: calculations for bispheres. Curves 2 (long dash): single scattering + incoherent double scattering + interference of light scattered once. Curves 3 (short dash): model 2 + interference of light scattered twice. Curve 4 (dash triple dot): model 3 + interference between the light scattered once and twice. Curves 5 (solid): exact calculations. Curves 6 (dot dash): model 3 but without near-field effects (note that the negative branch of polarization almost vanishes).

Let us now consider the scattering properties of clusters composed of a large number of monomers and discuss how these properties depend on the number of monomers, their refractive index, and packing density. Aggregates

producing a negative branch of polarization in the backscattering region will be of special interest, because this part of the angular dependence of polarization is important for the interpretation of observational data for various objects. Figure 8 shows the aggregate structures used for the scattering simulations. Clusters 1 have a tetrahedron lattice and the CPs are placed adjacent to each other in the grid points. The overall shape of the cluster is close to spherical. This is the most compact aggregate considered in this work. Clusters 2 also have a tetrahedron lattice, but no condition for equidimensional shape was imposed. Several more CPs were put on their otherwise compact surfaces. They preserve the tetrahedron lattice but otherwise where added randomly. Note that cluster 2 turned out to be more compact in its 50-CP version than in the 100-CP one. This causes an additional peculiarity of the polarization (see below). Clusters 3, 5, and 6 were generated by the diffusion-limited aggregation method [35]. Rather compact random clusters 4 were generated by the ballistic particle-cluster aggregation method [36]. The fractal dimensions and the pre-factors are also indicated in Fig. 8 together with the gyration radius R_g for each cluster. The gyration radius of clusters 4 is somewhat larger than those of clusters 2 and 3 and somewhat smaller than those of the sparse aggregates 5 and 6.

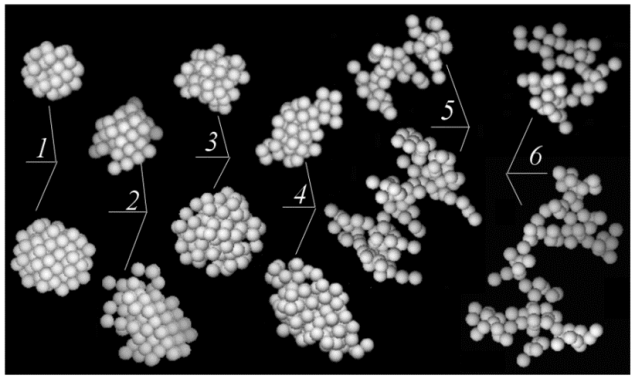

d_f			3.0	2.8	2.1	1.9
k_f			8.0	7.4	6.0	4.8
R_g	4.05	5.03	4.64	5.07	7.64	9.89

Figure 8: The aggregates composed of 50 (top) and 100 (bottom) CPs used in the model calculations. The first two are regular and have a tetrahedron lattice, the others are random fractals with different packing parameters (see text for details). The fractal dimensions, prefactors, and gyration radii (for 100 CPs) are shown in the footnote.

Our numerous calculations for various clusters with a moderate number of CPs and with the real part of the refractive index ranging from 1.4 to 1.9 show that the negative polarization branch at $\vartheta > 150°$ can be produced by compact aggregate structures with CP size parameters $0.7 < \tilde{x} < 2$ depending on $\mathrm{Re}(\tilde{m})$. However, the cluster structure is of significant importance. For

example, for the clusters composed of CPs with $\tilde{x}=1.5$ the value of the polarization inversion angle can vary within a 15° -wide range depending on specific cluster structure. This is probably caused by the interference of singly and doubly scattered waves. In what follows, we present only the results for $\tilde{x}=1.5$ and $\tilde{m}=1.65+0.05i$. (Note that the angular dependence of the degree of linear polarization for individual CPs with such properties is close to the Rayleigh one, i.e., the polarization is positive for all scattering angles and has a maximum of about 100% near $\vartheta=\pi/2$.) A detailed analysis of the optical properties of randomly oriented clusters composed of spherical particles, as well as the results for the other values of $\tilde{x}$ and $\tilde{m}$ can be found in [28].

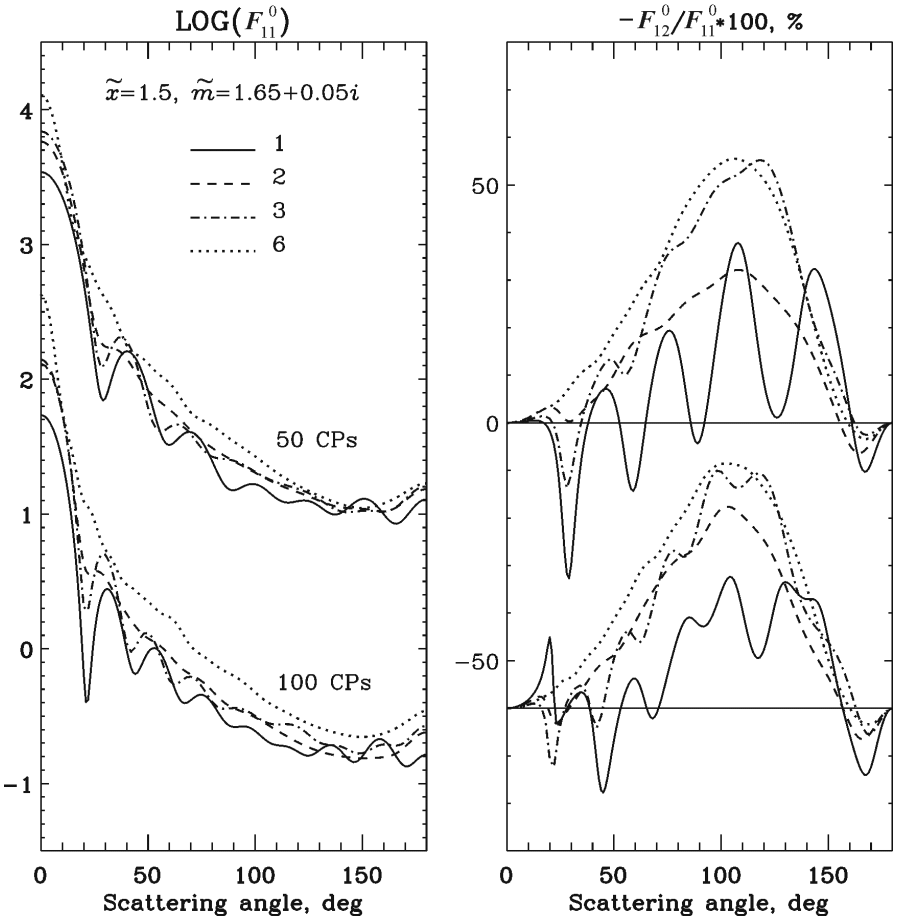

Figure 9: Intensity and polarization for aggregates of various types (1, 2, 3, and 6) consisting of 50 and 100 CPs with $\tilde{x}=1.5$ and $\tilde{m}=1.65+0.05i$. The sets of curves for 100 CPs are shifted down by 2.0 for intensity and by 60% for polarization.

A common feature of the aggregates considered is a significant decrease of polarization at side-scattering angles compared to the polarization of the individual CPs. As shown in [28], the increase of the real part of the refractive index strengthens this difference. This can be explained by both the multiple-

scattering contribution and the near-field effects.

The intensity and polarization of light scattered by four types of cluster (from those shown in Fig. 8) are displayed in Fig. 9 versus scattering angle. Although clusters 2 and 3 are also compact (like cluster 1), their scattering characteristics differ substantially from those of cluster 1, except at scattering angles 15°–40°, where similar behavior is observed for all three clusters. The difference is particularly evident in polarization. Some wavy behavior still appears in the curves for very compact random structures (cluster 3), especially for $\tilde{N} = 100$. However, the regular aggregate 2 with randomly added monomers on its outside shows a rather smooth angular dependence of the intensity and polarization. Similarly, if we add random monomers to the surface of a compact regular cluster (cluster 1) in such a way that each of them contacts only one of the CPs of the existing cluster, the interference structure in the curves of the intensity and polarization are damped. The influence of the structure of the surface layer of the aggregate on the scattering properties will be considered in detail below. The curves for the fluffy aggregate 6 show no oscillations. The polarization curve is bell-shaped like that of the individual CPs. However, the angular dependence for the aggregate has a much lower maximum (as compared to the polarization of the CP) and a negative branch at scattering angles close to the backscattering direction.

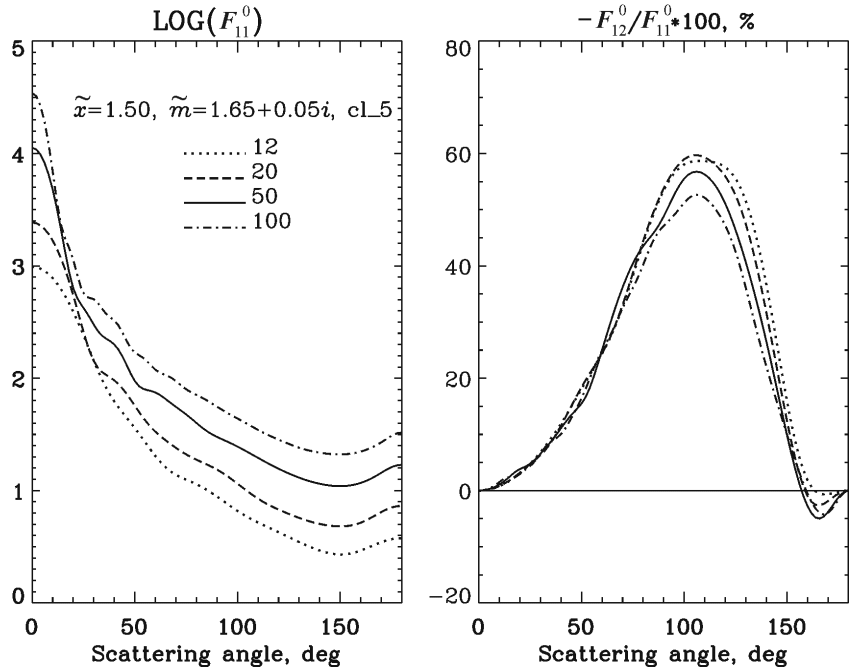

Figure 10: Dependence of intensity and polarization on the number of monomers (or cluster size) for cluster type 5 (see Fig. 8). The intensity increases, the polarization decreases, and the negative branch deepens with increasing the number of CPs.

It is worth noting that the sparse structures 5 and 6 are not very fluffy.

They contain rather compact blocks of CPs connected by chains. While the cluster as a whole determines the level of the intensity of the scattered light, which strongly depends on the cluster size, the blocks are responsible for generating polarization. This is well seen in Fig. 10, where the characteristics of type 5 clusters are displayed for an increasing number $\tilde{N}$ of CPs. The increase in $\tilde{N}$ depresses slightly the polarization maximum and strengthens the negative branch, although for larger $\tilde{N}$ the latter effect becomes less noticeable and the inversion angle remains almost unchanged.

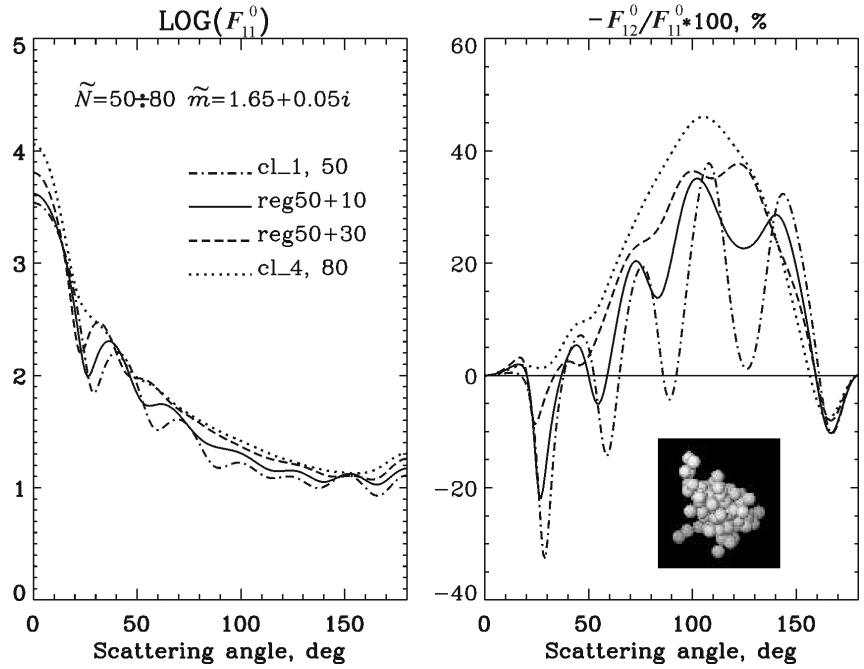

Figure 11: The intensity and polarization of light scattered by clusters with different structure of the surface layer. Additional CPs are placed in a random way on the outside of the completely regular compact cluster 1. The model for the random cluster 4 is also shown for comparison. The number of CPs is shown for each model. A picture of the aggregate after 30 CPs have been added to the surface is also shown.

Let us now consider the manifestations of the near-field effects in the scattering characteristics in more detail using clusters with different structure of the surface layer. These clusters have been generated in the following way. The compact regular aggregate of type 1 composed of 50 CPs served as a core. First, 10 CPs were added to its surface in a random way. Then 20 more CPs were added to the surface in the same way. The intensity and polarization of the original cluster and the two modified ones are displayed as functions of scattering angle in Fig. 11 and compared with those of a type 4 cluster consisting of 80 monomers. Even a few CPs added to the surface of the regular type 1 cluster significantly suppress the interference oscillations in the curves of the original type 1 cluster and make the curves to look similar to those of

the type 4 cluster with a more random structure. This can be explained as follows.

A layer of random particles added to the regular cluster works as an amplitude-phase inhomogeneity for the incident wave (see Fig. 5). After having passed through this layer, the wave becomes strongly inhomogeneous; the variations of its amplitude, phase, and propagation direction become chaotic. If the number of particles placed randomly in the outer layer is large enough, then there is almost no correlation between the phases of the radiation produced in the scattering of such a wave by the individual underlying particles. Consequently, the location of CPs deeper inside the cluster with respect to each other is unimportant for the scattering process. For the angular dependence of the intensity, the inner structure of the cluster is even less important. The intensity level increases with the number of CPs, albeit this growth also depends on the imaginary part of the refractive index [28]. The polarization produced in the scattering of inhomogeneous waves has been already considered in this section. Here we only note that, since the scattering properties of the inner CPs are not sensitive to their location, the polarization of the cluster depends only weakly on the number of CPs in the cluster and on the regularity of its inner structure, but more strongly on its packing density (see also Fig. 9).

In the backscattering region, the enhancement of intensity is formed by the CPs in the outer layer of the cluster, where the radiation field is practically homogeneous. At the same time, the negative polarization is also generated by the particles below the surface layer of the cluster, where the radiation field is inhomogeneous, and the amplitude, phase, and propagation direction of the wave change randomly. Note that the situation is the same in a powder-like layer, which makes conclusions also relevant to regolith surfaces. Thus, the field inhomogeneity below the surface layer of the cluster (or regolith) reduces the dependence of the negative polarization on the location of CPs in the deeper layers, but not on the compactness. Depending on the structure of the aggregate, the interference of multiply scattered waves or the near-field interactions are more efficient for a given cluster. This means that the opposition effects in intensity and polarization do not always go in parallel. That is, for the models in Fig. 10 the backscattering enhancement is almost the same for the clusters composed of 12 and 100 CPs, while the negative branch is weak for the small aggregate. For the compact regular clusters (Fig. 9), there is practically no backscattering enhancement, whereas the negative branch is more pronounced than for the sparse cluster.

5. Conclusions

We have presented the basic relations for electromagnetic scattering by ensembles of spherical particles and have demonstrated the differences in the description of the light scattering processes by sparse and closely packed

systems. In a low-density medium, the wave propagating from a scatterer to any neighbor is quasi-homogeneous. This allows the single-scattering characteristics of the individual particles to be used in describing the process of multiple scattering. We gave the equations quantifying the reflection from a plane-parallel layer of a sparse discrete random medium. One of them is a well-known vector radiative transfer equation; the second one describes the interference of multiply scattered waves resulting in the opposition effects. Numerical solutions of these equations show considerable dependence of the opposition effects on the properties of the medium and, specifically, on the microscopic characteristics of the scatterers.

In closely packed media, the waves in the vicinity of particles are inhomogeneous. Our qualitative analysis demonstrates that the wave inhomogeneity can lead to a suppression of the opposition effect in intensity and to causing (or strengthening) the negative polarization effect in the backscattering angular region. Computations for randomly oriented clusters show that the opposition effect in intensity and in the negative branch of polarization do not always appear simultaneously. Depending on the cluster structure, either the interference of multiply scattered waves or the near-field effects can play the decisive role.

6. Acknowledgments

V. Tishkovets, E. Petrova, and K. Jockers acknowledge the support of the Deusche Forschungsgemeinschaft in the framework of the priority program “Mars and the terrestrial planets” (Grant 436 RUS 113/684/0-1). The work by E. Petrova was supported in part by the RFBR Grant No. 01-02-17072. M. Mishchenko acknowledges support from the NASA Radiation Sciences Program managed by Donald Anderson.

References

1. M. P. van Albada and A. Lagendijk, Phys. Rev. Lett. **55**, 2692 (1985).
2. P. E. Wolf and G. Maret, Phys. Rev. Lett. **55**, 2696 (1985).
3. E. Akkermans, P. E. Wolf, R. Maynard R., and G. J. Maret, J. Phys. (Paris) **49**, 77 (1988).
4. M. P. van Albada, M. B. van der Mark, and A. Lagendijk, Phys. Rev. Lett. **58**, 361 (1987).
5. M. B. van der Mark, M. P. van Albada, and A. Lagendijk, Phys. Rev. B **37**, 3575 (1988).
6. B. Hapke, Icarus **88**, 407 (1990).
7. P. Sheng (Ed.), “Scattering and Localization of Classical Waves in Random Media” (World Scientific, Singapore, 1990).
8. K. Muinonen, Ph.D. thesis, Univ. Helsinki (1990).
9. Yu. G. Shkuratov, Astron. Vestnik **25**, 152 (1991).
10. M. I. Mishchenko and J. M. Dlugach, Mon. Not. R. Astron. Soc. **254**, 15P (1992).

11. M. I. Mishchenko and J. M. Dlugach, Planet. Space Sci. **41**, 173 (1993).
12. M. I. Mishchenko, Astrophys. J. **411**, 351 (1993).
13. A. Lagendijk and B. A. van Tiggelen, Phys. Rep. **270**, 143 (1996).
14. V. K. Rosenbush, V. V. Avramchuk, A. E. Rosenbush, and M. I. Mishchenko, Astrophys. J. **487**, 402 (1997).
15. R. S. Ruffine and D. A. De Wolf, J. Geophys. Res. **70**, 4313 (1965).
16. Yu. N. Barabanenkov, Yu. A. Kravtsov, V. D. Ozrin, and A. I. Saichev, Progr. Opt. **29**, 65 (1991).
17. V. L. Kuz'min and V. P. Romanov, Phys. Usp. **39**, 231 (1996).
18. M. I. Mishchenko, V. P. Tishkovets, and P. V. Litvinov, in G. Videen and M. Kocifaj (Eds.), "Optics of Cosmic Dust," p. 239 (Kluwer, Dordrecht, 2002).
19. V. D. Ozrin, Waves Random Media **2**, 141 (1992).
20. E. Amic, J. M. Luck, and Th. M. Nieuwenhuizen, J. Phys. I **7**, 445 (1997).
21. M. I. Mishchenko, J.-M. Luck, and T. M. Nieuwenhuizen, J. Opt. Soc. Am. A **17**, 888 (2000).
22. V. P. Tishkovets, J. Quant. Spectrosc. Radiat. Transfer **72**, 123 (2002).
23. V. P. Tishkovets, P. V. Litvinov, and M. V. Lyubchenko, J. Quant. Spectrosc. Radiat. Transfer **72**, 803 (2002).
24. V. P. Tishkovets, P. V. Litvinov, and S. V. Tishkovets, Opt. Spectrosc. **93**, 899 (2002).
25. V. P. Tishkovets and M. I. Mishchenko, J. Quant. Spectrosc. Radiat. Transfer (2004) (in press).
26. V. P. Tishkovets, Opt. Spectrosc. **85**, 212 (1998).
27. V. P. Tishkovets, Yu. G. Shkuratov, and P. V. Litvinov, J. Quant. Spectrosc. Radiat. Transfer **61**, 767 (1999).
28. V. P. Tishkovets, E. V. Petrova and K. Jockers, J. Quant. Spectrosc. Radiat. Transfer (2004) (in press).
29. M. I. Mishchenko, L. D. Travis, and A. A. Lacis, "Scattering, Absorption, and Emission of Light by Small Particles" (Cambridge University Press, Cambridge, 2002).
30. D. A. Varshalovich, A. N. Moskalev, and V. K. Khersonskii, "Quantum Theory of Angular Momentum" (World Scientific, Singapore, 1988).
31. B. U. Felderhof and R. B. Jones, J. Math. Phys. **28**, 836 (1987).
32. M. I. Mishchenko, J. Opt. Soc. Am. A **9**, 978 (1992).
33. P. V. Litvinov, V. P. Tishkovets, K. Muinonen, and G. Videen, in B. van Tiggelen and S. Skipetrov (Eds.), "Wave Scattering in Complex Media: From Theory to Applications," p. 567 (Kluwer, Dordrecht, 2003).
34. V. P. Tishkovets and P. V. Litvinov, Solar Syst. Res. **33,** 186 (1999).
35. R. Jullien and R. Botet, "Aggregation and Fractal Aggregates" (Singapore: World Scientific, 1987).
36. P. Meakin, J Colloid Interface Sci. **96**, 415 (1983).